Properties of Heavy Secondary Fluorine Cosmic Rays: Results from the Alpha Magnetic Spectrometer - SUPPLEMENTAL MATERIAL -

(AMS Collaboration)

For references see the main text.

Detector. — AMS is a general purpose high energy particle physics detector in space. The layout of the detector is shown in Fig. S1. The key elements are the permanent magnet, the silicon tracker, four planes of time of flight (TOF) scintillation counters, the array of antico-incidence counters (ACCs), a transition radiation detector (TRD), a ring imaging Čerenkov detector (RICH), and an electromagnetic calorimeter (ECAL). The three-dimensional imaging capability of the 17 radiation length ECAL allows for an accurate measurement of the energy E and the shower shape of $e^{\pm}$. The AMS coordinate system is concentric with the magnet. The x axis is parallel to the main component of the magnetic field and the z axis points vertically. The (y-z) plane is the bending plane. Above, below, and downward- going refer to the AMS coordinate system. The central field of the magnet is 1.4 kG. Before flight, the field was measured in 120 000 locations to an accuracy of better than 2 G. On orbit, the magnet temperature varies from -3 to $+20°$C. The field strength is corrected with a measured temperature dependence of $-0.09\%/°$C. The tracker has nine layers, the first ($L1$) at the top of the detector, the second ($L2$) just above the magnet, six ($L3$ to $L8$) within the bore of the magnet, and the last ($L9$) just above the ECAL. $L2$ to $L8$ constitute the inner tracker. Each layer contains double-sided silicon microstrip detectors which independently measure the x and y coordinates. The tracker accurately determines the trajectory of cosmic rays by multiple measurements of the coordinates with a resolution in each layer of 8 μm for fluorine nuclei in the bending (y) direction. Together, the tracker and the magnet measure the rigidity R of charged cosmic rays, with a maximum detectable rigidity of 2.9 TV for fluorine nuclei over the 3 m lever arm from $L1$ to $L9$.

Each layer of the tracker provides an independent measurement of the charge Z with a resolution of $\sigma_Z/Z = 3.0\%$ for fluorine nuclei. Overall, the inner tracker has a resolution of $\sigma_Z/Z = 1.3\%$.

As seen from Fig. S1, two of the TOF planes are located above the magnet (upper TOF) and two planes are below the magnet (lower TOF). The overall velocity ($\beta = v/c$) resolution has been measured to be $\sigma(1/\beta) = 0.01$ for fluorine nuclei. This discriminates between upward- and downward-going particles. The pulse heights of the two upper planes are combined to provide an independent measurement of the charge with an accuracy $\sigma_Z/Z = 2\%$. The pulse heights from the two lower planes are combined to provide another independent charge measurement with the same accuracy.

Fluorine nuclei traversing AMS were triggered as described in Ref. [24]. The trigger efficiency for the fluorine nuclei has been measured to be $>95\%$ over the entire rigidity range.

Monte Carlo (MC) simulated events were produced using a dedicated program developed by the collaboration based on the GEANT4-10.3 package [21]. The program simulates electromagnetic and hadronic [22] interactions of particles in the material of AMS and generates detector responses. The digitization of the signals is simulated precisely according to the measured characteristics of the electronics. The simulated events then undergo the same reconstruction as used for the data.

Event Selection. — In the first 8.5 years AMS has collected 1.50×10^{11} cosmic ray events. The collection time used in this analysis includes only those seconds during which the detector was in normal operating conditions and, in addition, AMS was pointing within $40°$ of the local zenith and the ISS was outside of the South Atlantic Anomaly. Due to the geomagnetic field, this collection time increases with rigidity, reaching 1.98×10^8 s above 30 GV.

Fluorine events are required to be downward going and to have a reconstructed track in the inner tracker which passes through $L1$. In the highest rigidity region, $R \geq 1.2$ TV, the track is also required to pass through $L9$. Track fitting quality criteria such as a $\chi^2/\text{d.o.f.} < 10$ in the bending coordinate are applied.

Charge measurements on $L1$, the inner tracker, the upper TOF, the lower TOF, and, for $R > 1.2$ TV, $L9$ are required to be compatible with charge $Z = 9$.

The measured rigidity is required to be greater than a factor of 1.2 times the maximum geomagnetic cutoff within the AMS field of view. The cutoff was calculated by backtracing [26] from the top of AMS out to 50 Earth's radii using the most recent International Geomagnetic Reference Field model [27].

Results.— To ensure that the choice of the inflection point of 175 GV in Eq. (4) does not affect the fit results, we allowed the inflection point (R_0) to vary, so the variation with rigidity of the spectral index Δ of F/Si flux ratio was obtained by fitting it with

$$\text{F/Si} = \begin{cases} C\,(R/R_0)^{\Delta_1}, & R \leq R_0, \\ C\,(R/R_0)^{\Delta_2}, & R > R_0. \end{cases} \tag{S1}$$

over the rigidity interval [28.8–2900] GV. The fit yields $C = 0.046 \pm 0.001$, $\Delta_1 = -0.35 \pm 0.03$, $\Delta_2 = -0.21 \pm 0.08$, and $R_0 = 150 \pm 61$ GV with $\chi^2/\text{d.o.f.} = 13/15$. Above 150 GV the F/Si spectral index Δ exhibits a hardening (Δ_2-Δ_1) of 0.14 ± 0.08, in complete agreement with the results of Eq. (4), $\Delta_2^{\text{F/Si}}$-$\Delta_1^{\text{F/Si}} = 0.015 \pm 0.07$.

TABLE SI: The F flux Φ as a function of rigidity at the top of AMS in units of $[\mathrm{m}^2 \cdot \mathrm{sr} \cdot \mathrm{s} \cdot \mathrm{GV}]^{-1}$ including errors due to statistics (stat.); contributions to the systematic error from the trigger and acceptance (acc.); the rigidity resolution function and unfolding (unf.); the absolute rigidity scale (scale); and the total systematic error (syst.). The contribution of individual sources to the systematic error are added in quadrature to arrive at the total systematic error.

Rigidity [GV]	Φ	$\sigma_{\text{stat.}}$	$\sigma_{\text{acc.}}$	$\sigma_{\text{unf.}}$	σ_{scale}	$\sigma_{\text{syst.}}$	
2.15 − 2.40	(2.956	0.042	0.108	0.052	0.014	0.121)	$\times 10^{-2}$
2.40 − 2.67	(2.739	0.035	0.097	0.036	0.008	0.104)	$\times 10^{-2}$
2.67 − 2.97	(2.576	0.030	0.089	0.028	0.004	0.093)	$\times 10^{-2}$
2.97 − 3.29	(2.342	0.026	0.079	0.021	0.002	0.082)	$\times 10^{-2}$
3.29 − 3.64	(2.099	0.022	0.070	0.016	0.000	0.072)	$\times 10^{-2}$
3.64 − 4.02	(1.824	0.018	0.060	0.012	0.001	0.061)	$\times 10^{-2}$
4.02 − 4.43	(1.537	0.015	0.050	0.008	0.001	0.051)	$\times 10^{-2}$
4.43 − 4.88	(1.305	0.012	0.043	0.006	0.002	0.043)	$\times 10^{-2}$
4.88 − 5.37	(1.085	0.010	0.035	0.004	0.002	0.036)	$\times 10^{-2}$
5.37 − 5.90	(8.940	0.083	0.290	0.032	0.017	0.292)	$\times 10^{-3}$
5.90 − 6.47	(7.382	0.069	0.239	0.024	0.015	0.241)	$\times 10^{-3}$
6.47 − 7.09	(6.026	0.056	0.195	0.018	0.014	0.197)	$\times 10^{-3}$
7.09 − 7.76	(4.879	0.046	0.158	0.014	0.012	0.159)	$\times 10^{-3}$
7.76 − 8.48	(3.949	0.038	0.128	0.011	0.010	0.129)	$\times 10^{-3}$
8.48 − 9.26	(3.206	0.031	0.104	0.009	0.009	0.105)	$\times 10^{-3}$
9.26 − 10.1	(2.609	0.027	0.085	0.007	0.007	0.085)	$\times 10^{-3}$
10.1 − 11.0	(2.107	0.023	0.069	0.006	0.006	0.069)	$\times 10^{-3}$
11.0 − 12.0	(1.663	0.019	0.054	0.005	0.005	0.055)	$\times 10^{-3}$
12.0 − 13.0	(1.349	0.017	0.044	0.004	0.004	0.044)	$\times 10^{-3}$
13.0 − 14.1	(1.097	0.014	0.036	0.003	0.004	0.036)	$\times 10^{-3}$
14.1 − 15.3	(8.896	0.120	0.290	0.026	0.029	0.293)	$\times 10^{-4}$
15.3 − 16.6	(7.140	0.101	0.233	0.022	0.024	0.235)	$\times 10^{-4}$
16.6 − 18.0	(5.701	0.085	0.186	0.018	0.020	0.188)	$\times 10^{-4}$
18.0 − 19.5	(4.509	0.071	0.147	0.015	0.016	0.149)	$\times 10^{-4}$
19.5 − 21.1	(3.646	0.059	0.119	0.012	0.013	0.121)	$\times 10^{-4}$
21.1 − 22.8	(2.915	0.049	0.096	0.010	0.011	0.097)	$\times 10^{-4}$
22.8 − 24.7	(2.453	0.041	0.081	0.009	0.009	0.082)	$\times 10^{-4}$
24.7 − 26.7	(1.870	0.033	0.062	0.007	0.007	0.063)	$\times 10^{-4}$
26.7 − 28.8	(1.514	0.028	0.050	0.006	0.006	0.051)	$\times 10^{-4}$
28.8 − 33.5	(1.078	0.015	0.036	0.004	0.004	0.036)	$\times 10^{-4}$
33.5 − 38.9	(7.054	0.113	0.238	0.031	0.029	0.241)	$\times 10^{-5}$
38.9 − 45.1	(4.624	0.085	0.157	0.022	0.020	0.160)	$\times 10^{-5}$
45.1 − 52.2	(2.989	0.064	0.103	0.015	0.014	0.105)	$\times 10^{-5}$
52.2 − 60.3	(1.923	0.048	0.067	0.010	0.009	0.068)	$\times 10^{-5}$
60.3 − 69.7	(1.200	0.035	0.042	0.007	0.006	0.043)	$\times 10^{-5}$
69.7 − 80.5	(7.771	0.261	0.275	0.047	0.042	0.282)	$\times 10^{-6}$
80.5 − 93.0	(5.176	0.198	0.185	0.033	0.030	0.190)	$\times 10^{-6}$
93.0 − 108	(2.986	0.137	0.108	0.020	0.019	0.111)	$\times 10^{-6}$

Table continued

Rigidity [GV]	Φ	$\sigma_{\text{stat.}}$	$\sigma_{\text{acc.}}$	$\sigma_{\text{unf.}}$	σ_{scale}	$\sigma_{\text{syst.}}$	
108 − 125	(2.227	0.111	0.081	0.016	0.015	0.084)	$\times 10^{-6}$
125 − 147	(1.437	0.078	0.053	0.011	0.011	0.055)	$\times 10^{-6}$
147 − 175	(7.765	0.508	0.289	0.064	0.067	0.303)	$\times 10^{-7}$
175 − 211	(4.421	0.338	0.167	0.043	0.044	0.178)	$\times 10^{-7}$
211 − 259	(2.701	0.228	0.103	0.033	0.032	0.113)	$\times 10^{-7}$
259 − 330	(1.498	0.140	0.058	0.024	0.022	0.067)	$\times 10^{-7}$
330 − 441	(6.123	0.716	0.246	0.148	0.120	0.311)	$\times 10^{-8}$
441 − 660	(2.218	0.307	0.093	0.089	0.063	0.143)	$\times 10^{-8}$
660 − 1200	(0.578	0.100	0.027	0.045	0.028	0.060)	$\times 10^{-8}$
1200 − 2900	(0.038	0.035	0.003	0.003	0.003	0.005)	$\times 10^{-8}$

TABLE SII: The fluorine to boron flux ratio F/B as a function of rigidity including errors due to statistics (stat.); contributions to the systematic error from the trigger, acceptance, and background (acc.); the rigidity resolution function and unfolding (unf.); the absolute rigidity scale (scale); and the total systematic error (syst.). The statistical errors are the sum in quadrature of the relative fluorine flux statistical errors and the relative boron flux statistical errors, multiplied by the F/B flux ratio. The systematic errors from the background subtraction, the trigger, and the event reconstruction and selection are likewise added in quadrature. The correlations in the systematic errors from the uncertainty in nuclear interaction cross sections, the unfolding, and the absolute rigidity scale between the fluorine and boron fluxes have been taken into account in calculating the corresponding systematic errors of the F/B flux ratio. The contribution of individual sources to the systematic error are added in quadrature to arrive at the total systematic uncertainty.

Rigidity [GV]	F/B	$\sigma_{\text{stat.}}$	$\sigma_{\text{acc.}}$	$\sigma_{\text{unf.}}$	σ_{scale}	$\sigma_{\text{syst.}}$
2.15 − 2.40	0.0595	0.0009	0.0037	0.0009	0.0001	0.0038
2.40 − 2.67	0.0570	0.0008	0.0033	0.0006	0.0000	0.0033
2.67 − 2.97	0.0581	0.0007	0.0031	0.0005	0.0000	0.0031
2.97 − 3.29	0.0590	0.0007	0.0030	0.0005	0.0000	0.0030
3.29 − 3.64	0.0600	0.0006	0.0029	0.0004	0.0000	0.0029
3.64 − 4.02	0.0601	0.0006	0.0028	0.0003	0.0000	0.0028
4.02 − 4.43	0.0594	0.0006	0.0026	0.0003	0.0000	0.0027
4.43 − 4.88	0.0602	0.0006	0.0026	0.0002	0.0000	0.0026
4.88 − 5.37	0.0601	0.0006	0.0026	0.0002	0.0000	0.0026
5.37 − 5.90	0.0602	0.0006	0.0025	0.0002	0.0000	0.0025
5.90 − 6.47	0.0607	0.0006	0.0025	0.0002	0.0000	0.0025
6.47 − 7.09	0.0609	0.0006	0.0025	0.0002	0.0000	0.0025
7.09 − 7.76	0.0614	0.0006	0.0025	0.0002	0.0000	0.0025
7.76 − 8.48	0.0614	0.0006	0.0025	0.0002	0.0000	0.0025
8.48 − 9.26	0.0618	0.0006	0.0025	0.0002	0.0000	0.0025
9.26 − 10.1	0.0629	0.0007	0.0025	0.0002	0.0000	0.0025
10.1 − 11.0	0.0631	0.0007	0.0025	0.0002	0.0000	0.0025
11.0 − 12.0	0.0625	0.0007	0.0025	0.0002	0.0000	0.0025
12.0 − 13.0	0.0634	0.0008	0.0025	0.0002	0.0000	0.0026
13.0 − 14.1	0.0643	0.0008	0.0026	0.0002	0.0001	0.0026
14.1 − 15.3	0.0650	0.0009	0.0026	0.0002	0.0001	0.0026
15.3 − 16.6	0.0653	0.0009	0.0026	0.0002	0.0001	0.0026
16.6 − 18.0	0.0660	0.0010	0.0027	0.0002	0.0001	0.0027
18.0 − 19.5	0.0648	0.0010	0.0026	0.0002	0.0001	0.0026
19.5 − 21.1	0.0658	0.0011	0.0027	0.0002	0.0001	0.0027
21.1 − 22.8	0.0661	0.0011	0.0027	0.0002	0.0001	0.0027
22.8 − 24.7	0.0700	0.0012	0.0028	0.0002	0.0001	0.0029
24.7 − 26.7	0.0669	0.0012	0.0027	0.0002	0.0001	0.0027
26.7 − 28.8	0.0678	0.0013	0.0028	0.0002	0.0001	0.0028
28.8 − 33.5	0.0679	0.0010	0.0028	0.0002	0.0001	0.0028
33.5 − 38.9	0.0696	0.0012	0.0029	0.0003	0.0001	0.0029
38.9 − 45.1	0.0723	0.0014	0.0030	0.0003	0.0001	0.0031

Table continued

Rigidity [GV]	F/B	$\sigma_{\text{stat.}}$	$\sigma_{\text{acc.}}$	$\sigma_{\text{unf.}}$	σ_{scale}	$\sigma_{\text{syst.}}$
45.1 − 52.2	0.0726	0.0016	0.0031	0.0003	0.0001	0.0031
52.2 − 60.3	0.0725	0.0019	0.0031	0.0003	0.0001	0.0031
60.3 − 69.7	0.0712	0.0021	0.0031	0.0004	0.0001	0.0031
69.7 − 80.5	0.0725	0.0025	0.0032	0.0004	0.0001	0.0032
80.5 − 93.0	0.0750	0.0030	0.0034	0.0004	0.0001	0.0034
93.0 − 108	0.0697	0.0033	0.0032	0.0004	0.0001	0.0032
108 − 125	0.0805	0.0041	0.0037	0.0006	0.0001	0.0038
125 − 147	0.0844	0.0047	0.0040	0.0007	0.0001	0.0040
147 − 175	0.0759	0.0051	0.0036	0.0007	0.0001	0.0037
175 − 211	0.0745	0.0059	0.0036	0.0009	0.0001	0.0037
211 − 259	0.0810	0.0071	0.0040	0.0012	0.0001	0.0042
259 − 330	0.0901	0.0087	0.0046	0.0017	0.0001	0.0049
330 − 441	0.0779	0.0094	0.0040	0.0020	0.0001	0.0045
441 − 660	0.0793	0.0113	0.0042	0.0032	0.0002	0.0053
660 − 1200	0.0775	0.0139	0.0044	0.0057	0.0004	0.0073
1200 − 2900	0.0458	0.0431	0.0041	0.0033	0.0004	0.0053

TABLE SIII: The fluorine to silicon flux ratio F/Si as a function of rigidity including errors due to statistics (stat.); contributions to the systematic error from the trigger, acceptance, and background (acc.); the rigidity resolution function and unfolding (unf.); the absolute rigidity scale (scale); and the total systematic error (syst.). The statistical errors are the sum in quadrature of the relative fluorine flux statistical errors and the relative silicon flux statistical errors, multiplied by the F/Si flux ratio. The systematic errors from the background subtraction, the trigger, and the event reconstruction and selection are likewise added in quadrature. The correlations in the systematic errors from the uncertainty in nuclear interaction cross sections, the unfolding, and the absolute rigidity scale between the fluorine and silicon fluxes have been taken into account in calculating the corresponding systematic errors of the F/Si flux ratio. The contribution of individual sources to the systematic error are added in quadrature to arrive at the total systematic uncertainty.

Rigidity [GV]	F/Si	$\sigma_{\text{stat.}}$	$\sigma_{\text{acc.}}$	$\sigma_{\text{unf.}}$	σ_{scale}	$\sigma_{\text{syst.}}$
2.15 − 2.40	0.1350	0.0020	0.0050	0.0056	0.0000	0.0075
2.40 − 2.67	0.1338	0.0018	0.0048	0.0026	0.0000	0.0055
2.67 − 2.97	0.1374	0.0017	0.0048	0.0016	0.0000	0.0051
2.97 − 3.29	0.1392	0.0017	0.0048	0.0014	0.0000	0.0050
3.29 − 3.64	0.1401	0.0016	0.0048	0.0012	0.0000	0.0049
3.64 − 4.02	0.1400	0.0015	0.0047	0.0010	0.0000	0.0048
4.02 − 4.43	0.1371	0.0015	0.0046	0.0009	0.0000	0.0047
4.43 − 4.88	0.1348	0.0014	0.0045	0.0008	0.0000	0.0046
4.88 − 5.37	0.1331	0.0013	0.0044	0.0007	0.0000	0.0045
5.37 − 5.90	0.1304	0.0013	0.0044	0.0006	0.0000	0.0044
5.90 − 6.47	0.1275	0.0013	0.0043	0.0005	0.0000	0.0043
6.47 − 7.09	0.1246	0.0012	0.0042	0.0005	0.0000	0.0042
7.09 − 7.76	0.1205	0.0012	0.0040	0.0004	0.0000	0.0041
7.76 − 8.48	0.1191	0.0012	0.0040	0.0004	0.0000	0.0040
8.48 − 9.26	0.1157	0.0012	0.0039	0.0004	0.0000	0.0039
9.26 − 10.1	0.1142	0.0012	0.0038	0.0004	0.0000	0.0038
10.1 − 11.0	0.1118	0.0013	0.0038	0.0004	0.0000	0.0038
11.0 − 12.0	0.1079	0.0013	0.0036	0.0003	0.0000	0.0036
12.0 − 13.0	0.1061	0.0014	0.0036	0.0003	0.0000	0.0036
13.0 − 14.1	0.1038	0.0014	0.0035	0.0003	0.0000	0.0035
14.1 − 15.3	0.1028	0.0015	0.0035	0.0003	0.0000	0.0035
15.3 − 16.6	0.1001	0.0015	0.0034	0.0003	0.0000	0.0034
16.6 − 18.0	0.0980	0.0015	0.0033	0.0003	0.0000	0.0033
18.0 − 19.5	0.0943	0.0016	0.0032	0.0003	0.0000	0.0032
19.5 − 21.1	0.0922	0.0016	0.0031	0.0003	0.0000	0.0031
21.1 − 22.8	0.0904	0.0016	0.0031	0.0003	0.0000	0.0031
22.8 − 24.7	0.0925	0.0016	0.0031	0.0003	0.0000	0.0032
24.7 − 26.7	0.0858	0.0016	0.0029	0.0003	0.0000	0.0029
26.7 − 28.8	0.0836	0.0016	0.0029	0.0003	0.0000	0.0029
28.8 − 33.5	0.0794	0.0012	0.0027	0.0003	0.0000	0.0028
33.5 − 38.9	0.0761	0.0013	0.0027	0.0003	0.0000	0.0027
38.9 − 45.1	0.0737	0.0014	0.0026	0.0003	0.0001	0.0026

Table continued

TABLE SIII – *(Continued).*

Rigidity [GV]	F/Si	$\sigma_{\text{stat.}}$	$\sigma_{\text{acc.}}$	$\sigma_{\text{unf.}}$	σ_{scale}	$\sigma_{\text{syst.}}$
45.1 − 52.2	0.0689	0.0015	0.0025	0.0003	0.0001	0.0025
52.2 − 60.3	0.0660	0.0017	0.0024	0.0003	0.0001	0.0024
60.3 − 69.7	0.0598	0.0018	0.0022	0.0003	0.0001	0.0022
69.7 − 80.5	0.0570	0.0020	0.0021	0.0003	0.0001	0.0021
80.5 − 93.0	0.0557	0.0022	0.0021	0.0003	0.0001	0.0021
93.0 − 108	0.0485	0.0023	0.0018	0.0003	0.0001	0.0019
108 − 125	0.0543	0.0028	0.0021	0.0003	0.0001	0.0021
125 − 147	0.0543	0.0030	0.0021	0.0004	0.0001	0.0021
147 − 175	0.0450	0.0030	0.0018	0.0003	0.0001	0.0018
175 − 211	0.0427	0.0033	0.0017	0.0004	0.0001	0.0017
211 − 259	0.0437	0.0038	0.0018	0.0005	0.0001	0.0018
259 − 330	0.0457	0.0044	0.0019	0.0006	0.0002	0.0020
330 − 441	0.0372	0.0044	0.0016	0.0008	0.0002	0.0018
441 − 660	0.0342	0.0048	0.0015	0.0012	0.0002	0.0020
660 − 1200	0.0333	0.0059	0.0017	0.0023	0.0003	0.0028
1200 − 2900	0.0162	0.0151	0.0013	0.0010	0.0003	0.0017
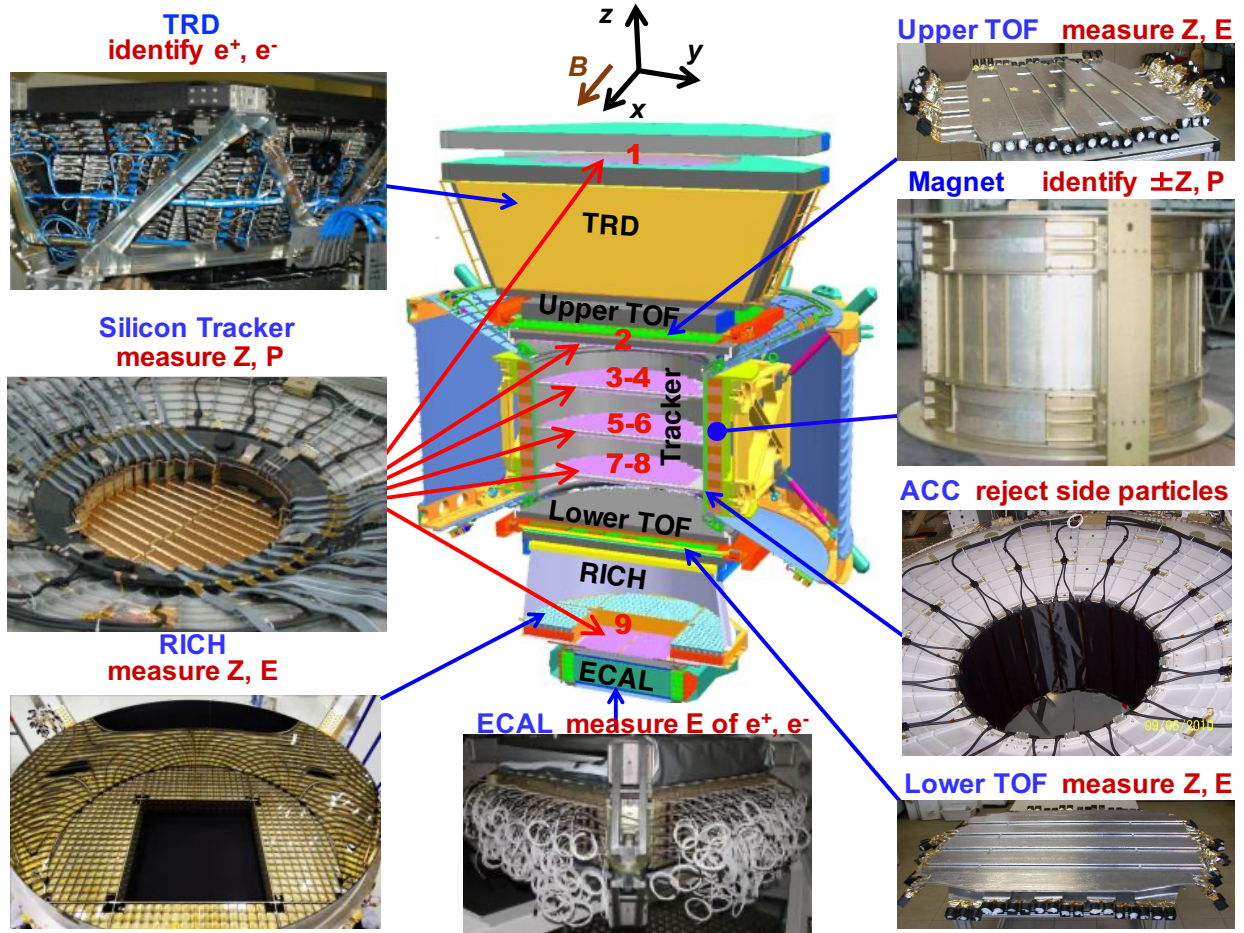
FIG. S1. The AMS detector showing the main elements and their functions. AMS is a TeV precision, multipurpose particle physics magnetic spectrometer in space. It identifies particles and nuclei by their charge Z, energy E and momentum P or rigidity ($R = P/Z$), which are measured independently by the Tracker, TOF, RICH and ECAL. The ACC counters, located in the magnet bore, are used to reject particles entering AMS from the side. The AMS coordinate system, concentric with the magnet, is also shown. The x axis is parallel to the main component of the magnetic field and the z axis is pointing vertically.
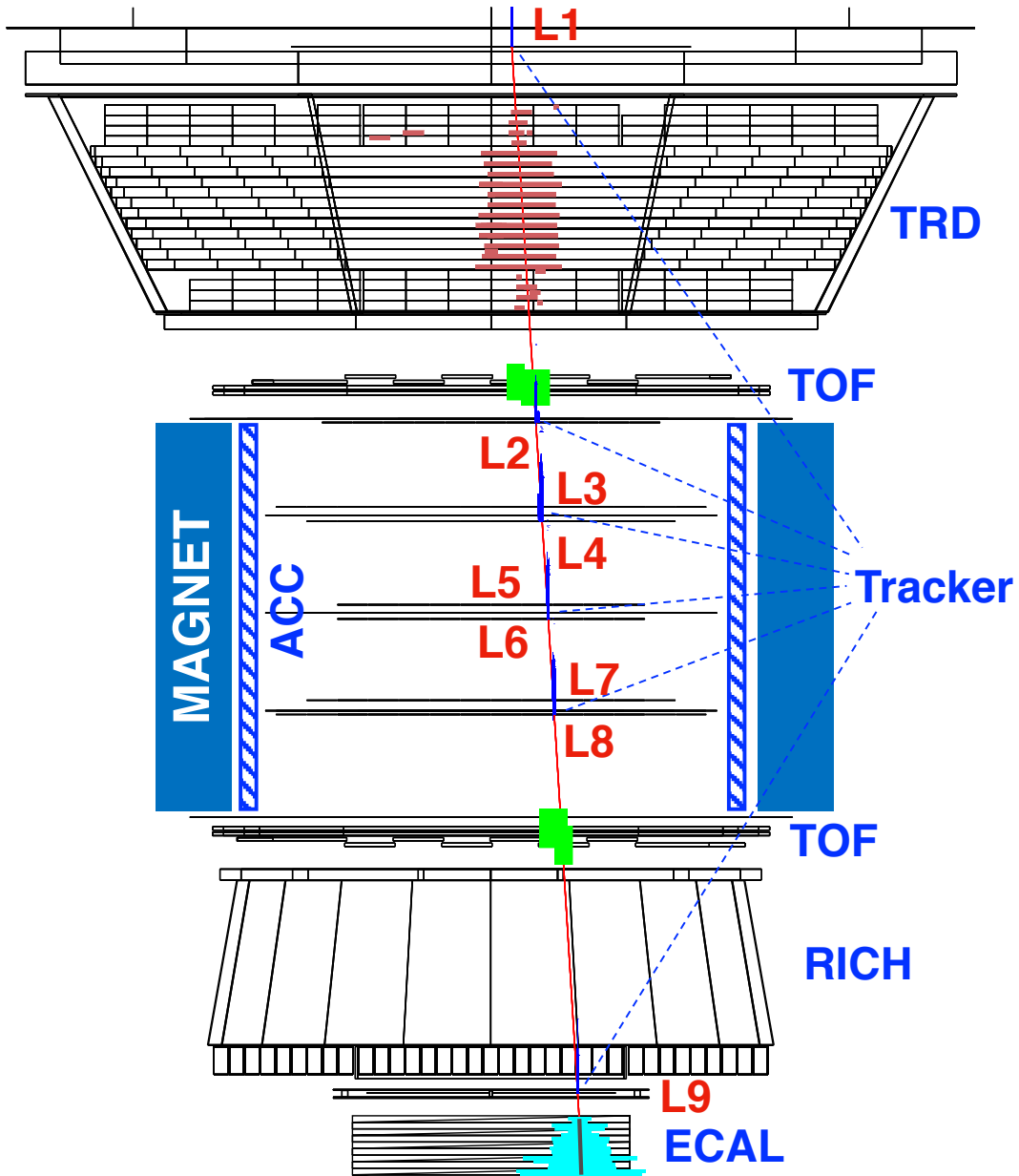
FIG. S2. An event display in the bending plane of a fluorine nuclei. The red line indicates the reconstructed trajectory. The magenta spread in TRD shows the dE/dx measurements in different TRD layers, green areas in upper and lower TOF carry the information of the dE/dx as well as the coordinate measurements. The vertical blue lines in the tracker layers carry the information of coordinates and dE/dx or pulse heights. The light blue area in ECAL shows the shower development. This downward-going event is identified as a fluorine Z=9 with $R = 26$ GV.
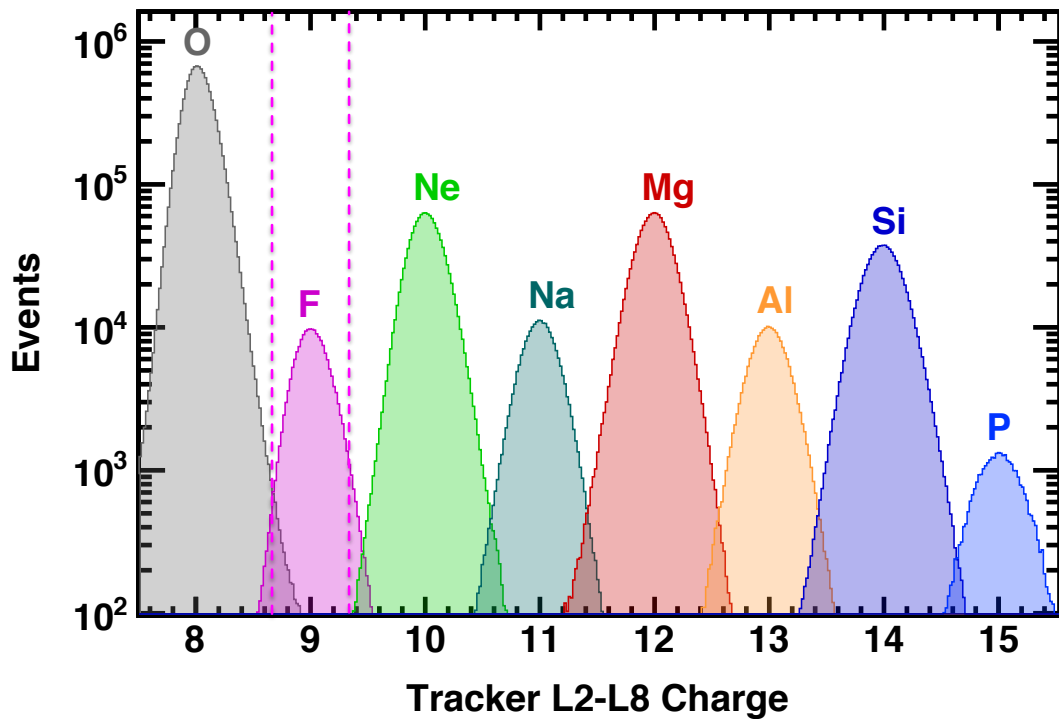
FIG. S3. Distribution of the charge measured with the inner tracker $L2$-$L8$ for samples from $Z = 8$ to $Z = 15$ selected by the combined charge measured with $L1$, the upper TOF, and the lower TOF over the rigidities above 4 GV. The dashed vertical lines correspond to the charge selection in the inner tracker for fluorine.
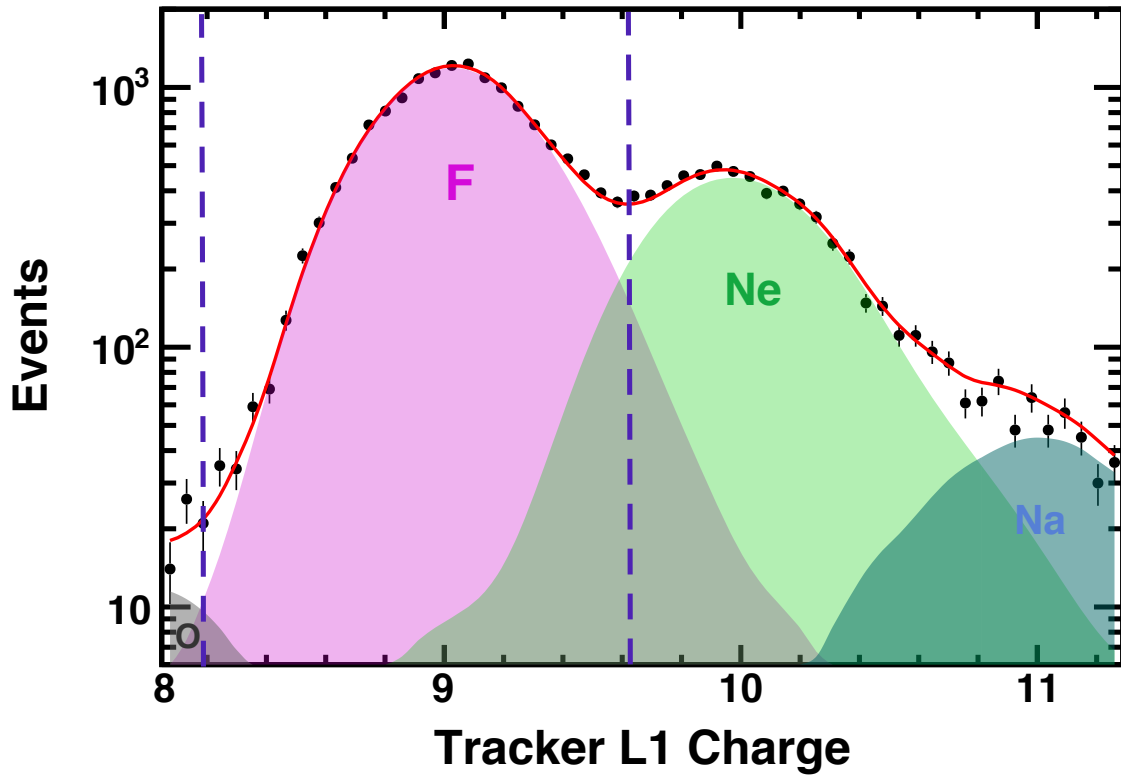
FIG. S4. Charge distributions measured by tracker $L1$ for fluorine events selected by the inner tracker $L2$-$L8$ in the rigidity range between 18 and 22 GV (black dots). The solid red curve shows the fit to the data of the sum of the O, F, Ne, and Na charge distribution templates. The templates are obtained from non-interacting samples at $L2$ by using combined $L1$, upper TOF, $L3$-$L8$, and lower TOF charge selections. The charge selection for F applied on tracker $L1$ is shown as vertical dashed lines.
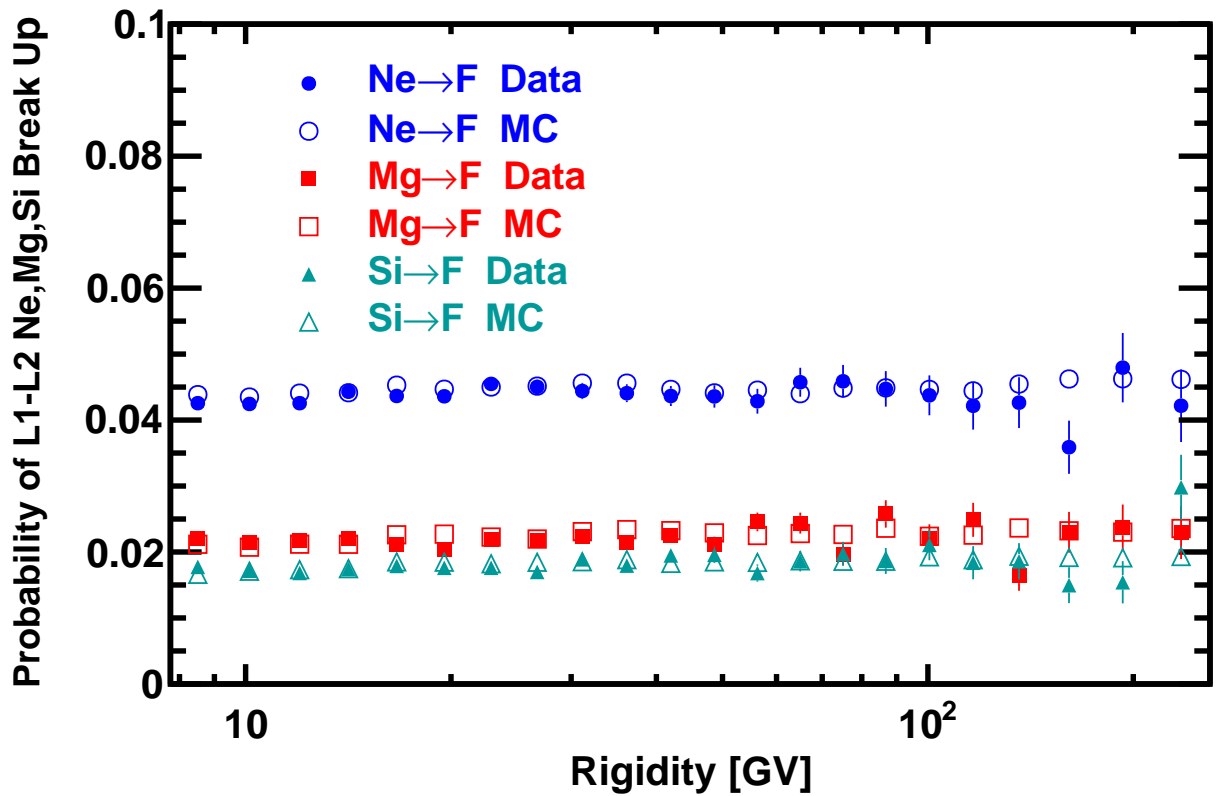
FIG. S5. Comparison of the simulated (MC) and measured (Data) Ne, Mg, Si→F break-up probabilities between $L1$ and $L2$.
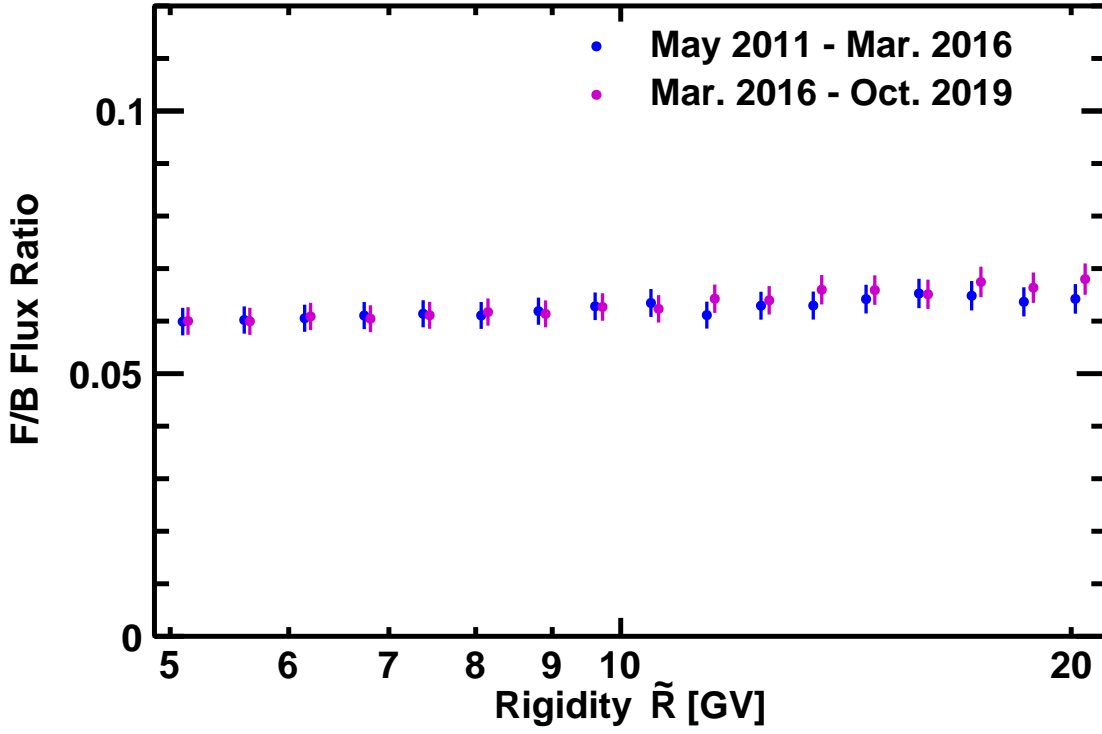
FIG. S6. The AMS F/B flux ratio from 5 to 20 GV for two different time periods, May 19, 2011 to March 3, 2016 (blue dots) and March 3, 2016 to October 30, 2019 (violet dots). For clarity, the data points are displaced horizontally. As seen, the F/B ratio does not depend on time, i.e. solar modulation of the F/B flux ratio does not affect the fit results with Eq. (3).
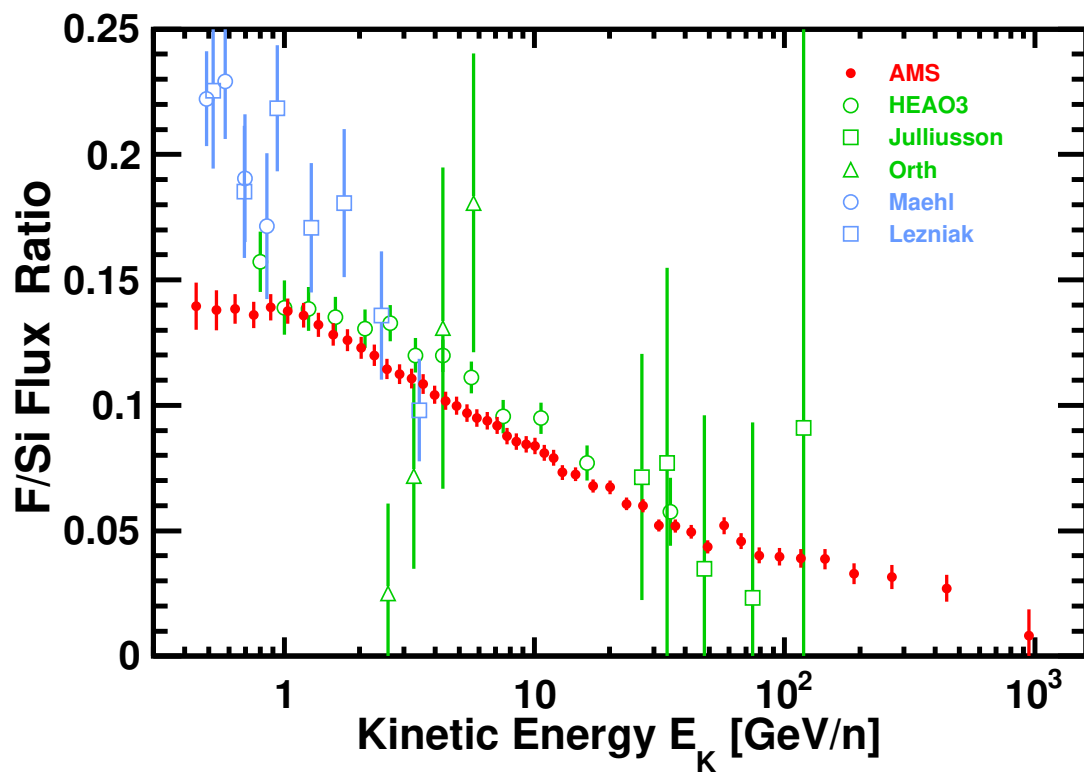
FIG. S7. The AMS F/Si flux ratio as a function of kinetic energy per nucleon E_K together with earlier measurements. For the conversion of AMS measurements from rigidity to kinetic energy per nucleon we used $^{19}_{9}\mathrm{F}$ and $^{28}_{14}\mathrm{Si}$.
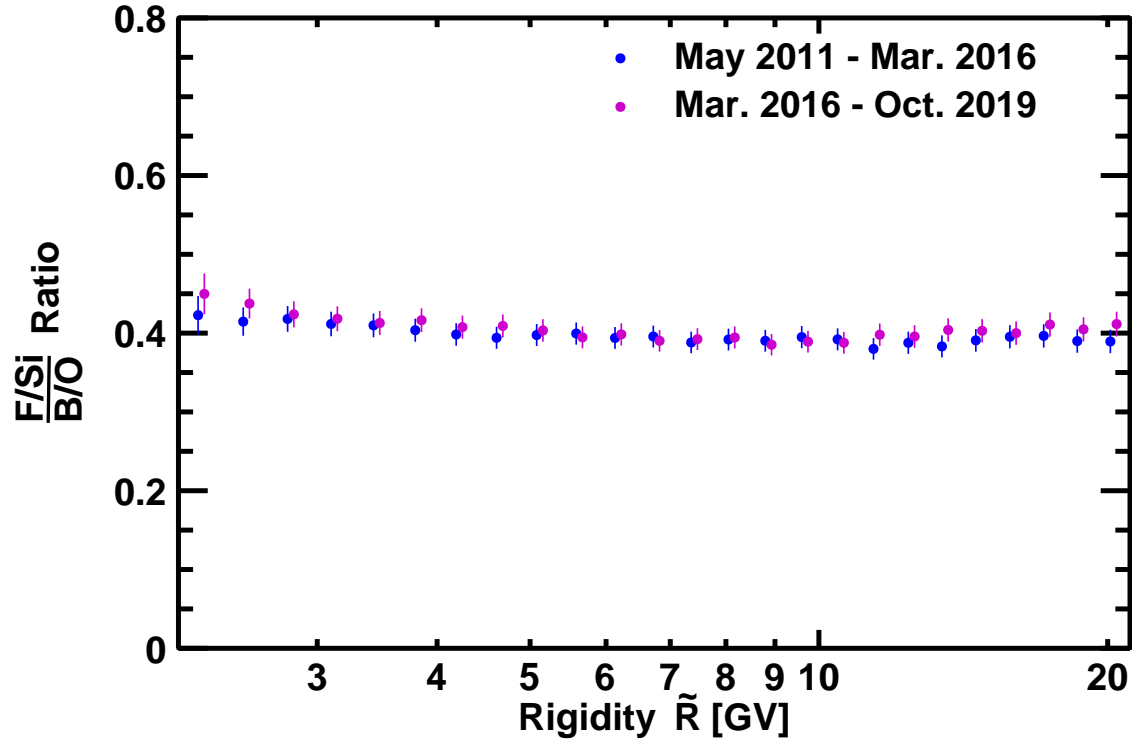
FIG. S8. The AMS $\frac{\mathrm{F/Si}}{\mathrm{B/O}}$ ratio below 20 GV for two different time periods, May 19, 2011 to March 3, 2016 (blue dots) and March 3, 2016 to October 30, 2019 (violet dots). For clarity, the data points are displaced horizontally. As seen, the $\frac{\mathrm{F/Si}}{\mathrm{B/O}}$ ratio does not depend on time, i.e. solar modulation of the $\frac{\mathrm{F/Si}}{\mathrm{B/O}}$ ratio does not affect the fit results with Eq. (5).